Research Article | Vol. 25, No. 21 | 16 Oct 2017 | OPTICS EXPRESS 25374
Optics EXPRESS

Mid-infrared light emission > 3 μm wavelength from tensile strained GeSn microdisks

R. W. Millar,[1] D. C. S. Dumas,[1] K. F. Gallacher, [1] P. Jahandar,[2] C. MacGregor, [3] M. Myronov [2,4] and D. J. Paul[1,*]

[1] *University of Glasgow, School of Engineering, Rankine Building, Oakfield Avenue, Glasgow, G12 8LT, UK*
[2] *Department of Physics, University of Warwick, Coventry, CV4 7AL, UK*
[3] *Gas Sensing Solutions, Cumbernauld, G68 9HQ, UK*
[4] *M.Myronov@warwick.ac.uk*
[*] *Douglas.Paul@glasgow.ac.uk*

Abstract: GeSn alloys with Sn contents of 8.4 % and 10.7 % are grown pseudomorphically on Ge buffers on Si (001) substrates. The alloys as-grown are compressively strained, and therefore indirect bandgap. Undercut GeSn on Ge microdisk structures are fabricated and strained by silicon nitride stressor layers, which leads to tensile strain in the alloys, and direct bandgap photoluminescence in the 3– 5 μm gas sensing window of the electromagnetic spectrum. The use of pseudomorphic layers and external stress mitigates the need for plastic deformation to obtain direct bandgap alloys. It is demonstrated, that the optically pumped light emission overlaps with the methane absorption lines, suggesting that GeSn alloys are well suited for mid-infrared integrated gas sensors on Si chips.

OCIS codes: 130.3060 Infrared; 160.3130 Integrated optics materials; 240.3990 Micro-optical devices; (000.2700); 280.4788 Optical sensing and sensors.

References and links

1. G. T. Reed, ed., *Silicon Photonics: The State of the Art* (John Wiley & Sons Ltd., 2008).
2. D. J. Paul, "Silicon photonics: a bright future?" Electron. Lett. **45**, 582–584 (2009).
3. J. Liu, X. Sun, R. Camacho-Aguilera, L. C. Kimerling, and J. Michel, "Ge-on-Si laser operating at room temperature," Opt. Lett. **35**, 679–681 (2010).
4. R. E. Camacho-Aguilera, Y. Cai, N. Patel, J. T. Bessette, M. Romagnoli, L. C. Kimerling, and J. Michel, "An electrically pumped germanium laser," Opt. Express **20**, 11316–11320 (2012).
5. M. V. Fischetti and S. E. Laux, "Band structure, deformation potentials, and carrier mobility in strained Si, Ge, and SiGe alloys," J. Appl. Phys. **80**, 2234 (1996).
6. M. J. Suess, R. Geiger, R. A. Minamisawa, G. Schiefler, J. Frigerio, D. Chrastina, G. Isella, R. Spolenak, J. Faist, and H. Sigg, "Analysis of enhanced light emission from highly strained germanium microbridges," Nat. Photonics **7**, 466–472 (2013).
7. D. S. Sukhdeo, D. Nam, J.-H. Kang, M. L. Brongersma, and K. C. Saraswat, "Direct bandgap germanium-on-silicon inferred from 57% <100> uniaxial tensile strain [Invited]," Photon. Res. **2**, A8 (2014).
8. J. Petykiewicz, D. Nam, D. S. Sukhdeo, S. Gupta, S. Buckley, A. Y. Piggott, J. Vučković, and K. C. Saraswat, "Direct bandgap light emission from strained germanium nanowires coupled with high-q nanophotonic cavities," Nano Letters **16**, 2168–2173 (2016).
9. G. Capellini, C. Reich, S. Guha, Y. Yamamoto, M. Lisker, M. Virgilio, A. Ghrib, M. E. Kurdi, P. Boucaud, B. Tillack, and T. Schroeder, "Tensile Ge microstructures for lasing fabricated by means of a silicon complementary metal-oxide-semiconductor process," Opt. Express **22**, 399–410 (2014).
10. R. Millar, K. Gallacher, A. Samarelli, J. Frigerio, D. Chrastina, G. Isella, T. Dieing, and D. Paul, "Extending the emission wavelength of Ge nanopillars to 2.25 μm using silicon nitride stressors," Opt. Express **23**, 18193–18202 (2015).
11. A. Ghrib, M. El Kurdi, M. Prost, S. Sauvage, X. Checoury, G. Beaudoin, M. Chaigneau, R. Ossikovski, I. Sagnes, and P. Boucaud, "All-Around SiN Stressor for High and Homogeneous Tensile Strain in Germanium Microdisk Cavities," Adv. Opt. Mater. **3**, 353–358 (2015).
12. M. El Kurdi, M. Prost, A. Ghrib, S. Sauvage, X. Checoury, G. Beaudoin, I. Sagnes, G. Picardi, R. Ossikovski, and P. Boucaud, "Direct band gap germanium microdisks obtained with silicon nitride stressor layers," ACS Photonics **3**, 443–448 (2016).

#302165 https://doi.org/10.1364/OE.25.025374
Journal © 2017 Received 14 Jul 2017; revised 21 Sep 2017; accepted 21 Sep 2017; published 5 Oct 2017

Optics EXPRESS

13. R. Millar, K. Gallacher, J. Frigerio, A. Ballabio, A. Bashir, I. MacLaren, G. Isella, and D. J. Paul, "Analysis of Ge micro-cavities with in-plane tensile strains above 2 %," Opt. Express **24**, 4365–4374 (2016).
14. Sanchez-Perez, J. R., Boztug, Cicek, Chen, Feng, Sudradjat, F. F., Paskiewicz, D. M., Jacobson, RB, Lagally, M. G., and R. Paiella, "Direct-bandgap light-emitting germanium in tensilely strained nanomembranes," Proc. Nat. Acad. Sci. **108**, 18893–18898 (2011).
15. D. S. Sukhdeo, D. Nam, J.-H. Kang, M. L. Brongersma, and K. C. Saraswat, "Bandgap-customizable germanium using lithographically determined biaxial tensile strain for silicon-compatible optoelectronics," Opt. Express **23**, 16740 (2015).
16. S. Wirths, R. Geiger, N. von den Driesch, G. Mussler, T. Stoica, S. Mantl, Z. Ikonic, M. Luysberg, S. Chiussi, J. M. Hartmann, H. Sigg, J. Faist, D. Buca, and D. Grützmacher, "Lasing in direct-bandgap GeSn alloy grown on Si," Nat. Photonics **9**, 88–92 (2015).
17. D. Stange, S. Wirths, R. Geiger, C. Schulte-Braucks, B. Marzban, N. V. D. Driesch, G. Mussler, T. Zabel, T. Stoica, J.-M. Hartmann, S. Mantl, Z. Ikonic, D. Grützmacher, H. Sigg, J. Witzens, and D. Buca, "Optically Pumped GeSn Microdisk Lasers on Si," ACS Photonics **3**, 1279–1285 (2016).
18. S. Al-Kabi, S. A. Ghetmiri, J. Margetis, T. Pham, Y. Zhou, W. Dou, B. Collier, R. Quinde, W. Du, A. Mosleh, J. Liu, G. Sun, R. A. Soref, J. Tolle, B. Li, M. Mortazavi, H. A. Naseem, and S.-Q. Yu, "An optically pumped 2.5 μm GeSn laser on Si operating at 110 K," Appl. Phys. Lett. **109**, 171105 (2016).
19. F. Pezzoli, F. Isa, G. Isella, C. Falub, T. Kreiliger, M. Salvalaglio, R. Bergamaschini, E. Grilli, M. Guzzi, H. von Känel, and L. Miglio, "Ge Crystals on Si Show Their Light," Phys. Rev. Appl. **1**, 044005 (2014).
20. F. Pezzoli, A. Giorgioni, D. Patchett, and M. Myronov, "Temperature-dependent photoluminescence characteristics of GeSn epitaxial layers," ACS Photonics **3**, 2004–2009 (2016).
21. S. Wirths, Z. Ikonic, A. T. Tiedemann, B. Holländer, T. Stoica, G. Mussler, U. Breuer, J. M. Hartmann, A. Benedetti, S. Chiussi, D. Grützmacher, S. Mantl, and D. Buca, "Tensely strained GeSn alloys as optical gain media," Appl. Phys. Lett. **103**, 0–5 (2013).
22. D. Sukhdeo, Y. Kim, S. Gupta, K. Saraswat, B. Dutt, and D. Nam, "Theoretical Modeling for the Interaction of Tin Alloying with N-Type Doping and Tensile Strain for GeSn Lasers," IEEE Electron Device Lett. **37**, 1307–1310 (2016).
23. J. Hodgkinson and R. P. Tatam, "Optical gas sensing: a review," Meas. Sci. Technol. **24**, 012004 (2013).
24. L. Rothman, I. Gordon, Y. Babikov, A. Barbe, D. C. Benner, P. Bernath, M. Birk, L. Bizzocchi, V. Boudon, L. Brown, A. Campargue, K. Chance, E. Cohen, L. Coudert, V. Devi, B. Drouin, A. Fayt, J.-M. Flaud, R. Gamache, J. Harrison, J.-M. Hartmann, C. Hill, J. Hodges, D. Jacquemart, A. Jolly, J. Lamouroux, R. L. Roy, G. Li, D. Long, O. Lyulin, C. Mackie, S. Massie, S. Mikhailenko, H. MÃijller, O. Naumenko, A. Nikitin, J. Orphal, V. Perevalov, A. Perrin, E. Polovtseva, C. Richard, M. Smith, E. Starikova, K. Sung, S. Tashkun, J. Tennyson, G. Toon, V. Tyuterev, and G. Wagner, "The hitran2012 molecular spectroscopic database," Journal of Quantitative Spectroscopy and Radiative Transfer **130**, 4 – 50 (2013). HITRAN2012 special issue.
25. R. Soref, "Mid-infrared photonics in silicon and germanium," Nat. Photonics **4**, 495–497 (2010).
26. D. Stange, S. Wirths, N. von den Driesch, G. Mussler, T. Stoica, Z. Ikonic, J. M. Hartmann, S. Mantl, D. Grützmacher, and D. Buca, "Optical Transitions in Direct-Bandgap $Ge_{1-x}Sn_x$ Alloys," ACS Photonics **2**, 1539–1545 (2015).
27. S. Gupta, R. Chen, Y. C. Huang, Y. Kim, E. Sanchez, J. S. Harris, and K. C. Saraswat, "Highly selective dry etching of germanium over germanium-tin ($Ge_{1-x}Sn_x$): A novel route for $Ge_{1-x}Sn_x$ nanostructure fabrication," Nano Lett. **13**, 3783–3790 (2013).
28. A. Ghrib, M. E. Kurdi, M. de Kersauson, M. Prost, S. Sauvage, X. Checoury, G. Beaudoin, I. Sagnes, and P. Boucaud, "Tensile-strained germanium microdisks," Appl. Phys. Lett. **102**, 221112 (2013).
29. C. S. Fenrich, X. Chen, R. Chen, Y. C. Huang, H. Chung, M. Y. Kao, Y. Huo, T. I. Kamins, and J. S. Harris, "Strained Pseudomorphic $Ge_{1-x}Sn_x$ Multiple Quantum Well Microdisk Using SiN_y Stressor Layer," ACS Photonics **3**, 2231–2236 (2016).
30. G. G. Stoney, "The tension of metallic films deposited by electrolysis," Proc. R. Soc. London, Ser. A **82**, 172–175 (1909).
31. S. Gupta, R. Chen, J. S. Harris, and K. C. Saraswat, "Atomic layer deposition of Al_2O_3 on germanium-tin (GeSn) and impact of wet chemical surface pre-treatment," Appl. Phys. Lett. **103**, 10–14 (2013).
32. R. Hickey, N. Fernando, S. Zollner, J. Hart, R. Hazbun, and J. Kolodzey, "Properties of pseudomorphic and relaxed $germanium_{1-x}$ tin_x alloys (x < 0.185) grown by MBE," Journal of Vacuum Science & Technology B, Nanotechnology and Microelectronics: Materials, Processing, Measurement, and Phenomena **35**, 021205 (2017).
33. R. Chen, H. Lin, Y. Huo, C. Hitzman, T. I. Kamins, J. S. Harris, R. Cheng, W. Wang, X. Gong, L. Sun, P. Guo, H. Hu, Z. Shen, G. Han, and Y.-C. Yeo, "Relaxed and Strained Patterned Germanium-Tin Structures: A Raman Scattering Study," ECS J. Solid State Sci. Technol. **2**, P138–P145 (2013).
34. F. Pezzoli, A. Giorgioni, K. Gallacher, F. Isa, P. Biagioni, R. W. Millar, E. Gatti, E. Grilli, E. Bonera, G. Isella, D. J. Paul, and L. Miglio, "Disentangling nonradiative recombination processes in Ge micro-crystals on Si substrates," Applied Physics Letters **108**, 262103 (2016).

Optics EXPRESS

1. Introduction

For the last decade, a number of research groups have focused on engineering Ge to create an efficient Group IV light source. The material is only indirect bandgap by ~ 140 meV, making the direct valley electrically accessible, however a large density of states (DOS) in the L-valley means that significant injection (or n-type doping) is required before carriers significantly populate the Γ-valley. [1, 2] While lasing has been demonstrated in degenerately doped n–Ge [3, 4], the free carrier and intra-valence band absorption caused by high injection led to high lasing thresholds. In order to reduce the required injection, a number of techniques have been employed, including the application of tensile strain and alloying with α-Sn. Increasing the tensile strain or Sn concentration lowers the Γ energy at a greater rate than the L-valley, therefore leading to a transition to a direct bandgap material. [5] High tensile strain has been demonstrated in Ge with suspended micro and nano-wires [6–8], which locally amplify the residual tensile strain in the epilayer, and through application of high stress silicon nitride (SiN) layers to optical cavities [9–13], amongst other techniques [14, 15]. Both these methods have induced levels of strain required for a transition to direct bandgap, however lasing has not been demonstrated from such devices.

Since overcoming a number of epitaxial growth challenges, direct bandgap GeSn alloys with 12.6 % Sn have been shown to be direct bandgap, and lasing has been demonstrated at low temperatures [16–18]. Lasing thresholds, however, remain large (>68 kW/cm^2), and strong thermal quenching is present above 110 K. [18] When grown on (100) Ge or Si substrates, GeSn alloys develop biaxial compressive strain, which partially counteracts the effect of the Sn alloying on the band-structure. This means that for the levels of Sn incorporation currently achievable for device grade alloys, there is an inherent need for strain relaxation in order to achieve a direct band-structure. In the GeSn lasers demonstrated so far, this strain relaxation has been through plastic deformation, and the formation of dislocation in > 300 nm thick layers. Such dislocations are highly undesirable as their inclusion leads to a reduction of non-radiative recombination lifetimes [19, 20], which is likely to partially account for the high thresholds observed in the lasers demonstrated so far.

In this work, strain engineering and Sn alloying techniques are combined, and high quality GeSn epitaxial layers are externally strained to produce tensile, direct bandgap alloys emitting in the mid-infrared (MIR). This is achieved without the need for plastic deformation and dislocation formation, which could be vital for producing low threshold GeSn lasers, or efficient light sources. Optical gain modelling has revealed that moderate tensile strain and Sn content could in fact provide higher gain than fully relaxed alloys with higher Sn concentrations [21, 22]. The techniques used here make use of GeSn epi-layers grown pseudomorphically on Ge relaxed buffers (on Si substrates), which ensures the alloys have minimal dislocations, with only threads penetrating from the underlying Ge buffer. A high strain transfer is achieved by applying high stress SiN layers to undercut GeSn/Ge microdisk structures.

Not only are the resultant tensile strained alloys direct bandgap, but the red-shift in emission associated with strain and Sn alloying shifts the room temperature emission into the 3- 5 μm sensing window of the electromagnetic spectrum; a first for GeSn light emitters. This development suggests that GeSn technologies have enormous potential for optical gas sensing, with pollution monitoring and healthcare applications [23]. Simulations demonstrate that the spectra from the highest strained $Ge_{0.893}Sn_{0.107}$ structures in this work have a good overlap with the methane absorption lines [24]. Tensile strained GeSn technologies can therefore potentially leverage Si foundry technologies to provide cheaper alternatives to III-V MIR light emitters and detectors. This technology could therefore complement a number of passive Group IV components that are being investigated for MIR applications [25], with the disks here being suitable for integration into Si, Ge or $Si_{1-x-y}Ge_xSn_y$ waveguide photonics with the potential for single-chip integrated sensors on a Si platform.

Optics EXPRESS

2. Growth and material properties

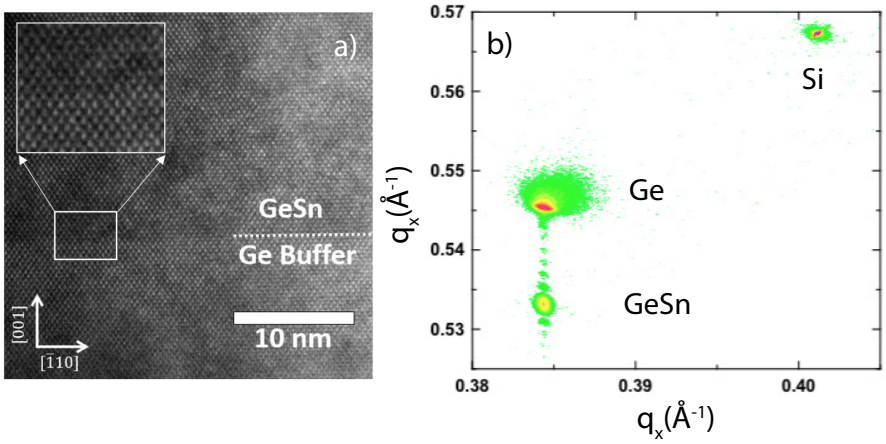

Fig. 1. a) A high resolution transmission electron microscope image showing the interface between a GeSn epilayer and a Ge relaxed buffer. b) X-ray diffraction reciprocal space map (XRD-RSM) of a pseudomorphic $Ge_{0.916}Sn_{0.084}$ layer on a Ge buffer, on a (001) Si substrate.

GeSn alloys with Sn contents of 8.4 % and 10.7 % were grown psuedomorphically on 650 nm thick relaxed Ge buffers, on (001) Si by reduced pressure - chemical vapour deposition (RP-CVD). Initially, the Ge buffers are grown using the two temperature technique, and thermally annealed at 830 °C in order to minimise the threading dislocation density (TDD). As shown in Fig. 1(a), a high quality interface is evident between the GeSn and Ge buffer layers. Due to the anneals, a small tensile strain of ~ 0.18 % accumulates in the Ge layer due to the difference in the thermal expansion coefficients of Ge and Si.

For the alloys, commercially available $SnCl_4$ and Ge_2H_6 precursors were used, with growth temperatures below 350 °C to minimise Sn segregation and diffusion. X-Ray diffraction (XRD) measurements about the (004) and (224) reflections were used to measure the in-plane and out of plane lattice constants of the grown structures, and therefore calculate the Sn concentrations. The alloys are sufficiently thin (~ 40 nm) that they are pseudomorphic to the Ge layer, and therefore there are minimal dislocations formed, due to the lack of strain relaxation. It was found, however, that threading dislocations stemming from the Ge buffer can penetrate the alloy. An XRD reciprocal space map for the $Ge_{0.916}Sn_{0.084}$ layer is shown in Fig. 1(b), showing the pseudomorphic growth. As grown, both alloys are calculated to be indirect bandgap, due to high compressive strains of 1.10 % and 1.44 % for the $Ge_{0.916}Sn_{0.084}$ and $Ge_{0.893}Sn_{0.107}$ layers respectively.

Given the discrepancy in the Γ and L-valley bandgap bowing parameters in the literature, it was experimentally verified that the two alloys demonstrated comparable behaviour in terms of the temperature dependence of the photoluminescence (PL), Fig. 2. This technique can highlight the direct or indirect nature of semiconductor materials, and is based on the fact that at low temperatures the Fermi-function approaches a step function, and electrons primarily occupy the the lowest energy states in the conduction band (assuming that they reach a quasi-equilibrium after injection).

If the Γ is the lowest energy band then the increased carrier occupation should result in significantly brighter PL, as it has a much higher quantum efficiency compared to indirect transitions. This is complicated, however, by the fact that indirect transitions can increase in

Optics EXPRESS

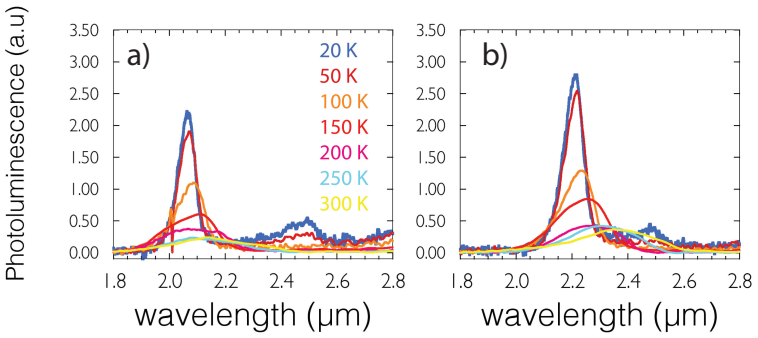

Fig. 2. a) Low temperature photoluminescence from 40 nm thick GeSn epilayers on 650 nm thick Ge buffers on (100) Si. a) 8.4 % Sn and (b) 10.7 % Sn concentrations. An artifact due to the optical chopper has been removed from the spectra.

intensity at low temperature as many non-radiative recombination mechanisms are significantly reduced. This was highlighted in recent work, which demonstrated that the temperature dependent PL from indirect GeSn layers is highly sensitive to the alloy relaxation and therefore on the defect density [20]. The technique, however, should still be valid in discriminating between indirect and direct bandgap layers of a comparable defect density.

Here, both alloys demonstrated a slight increase in the relative integrated PL intensity at 20 K compared to 300 K, by a factor of ~ 2.5 - 3. In both cases only one interband transition is observable throughout the measurement range. These results are extremely consistent with low defect density, indirect GeSn alloys with lower Sn concentrations [20]. It is therefore concluded that the PL from the as grown wafers demonstrates indirect, L $\rightarrow$ heavy-hole (HH) transitions, as the HH band is the ground state under compressive strain [2]. As shown in Fig. 2, at low temperatures, there is the emergence of a peak at around 2.5 μm, which is likely from dislocations that penetrate the alloy from the Ge buffer - a similar peak has previously been reported in pseudomorphic GeSn layers [26].

3. Fabrication

In order to provide high tensile strain at the top plane, undercut microdisk structures were fabricated using a combination of dry and wet etching techniques, Fig. 3(a,b), using processes described in [13]. The structures were patterned in mm-sized arrays by electron beam lithography, to facilitate low temperature PL measurements in an optical cryostat system. Here, the disks comprise GeSn/Ge layers, with a Si post, Fig. 3(c). By undercutting only the Ge buffer opposed to the GeSn epilayer, low damage wet etches can be used, opposed to selective dry etches [27]. Furthermore, when applying single layer SiN stressors, there is inherently compression at the bottom of the disk [28], therefore by undercutting the Ge virtual substrate (VS) it ensures a much more homogenous vertical strain distribution over the GeSn layer. With the Ge present there is a low defect interface (as shown in Fig. 1), with a type 1 band alignment at the Γ-valley that reduces diffusion into the Ge. This was thought to be preferable to having a free standing GeSn interface with potentially high surface recombination. The wet etch undercuts the disks by approximately 1.2 μm, as measured by scanning electron microscope (SEM) images, Fig. 3. Despite the difference in thickness between the GeSn layer and the Ge buffer, there is more elastic energy in the alloy than the moderately strained Ge buffer layer. For the $Ge_{0.893}Sn_{0.107}$ ($Ge_{0.916}Sn_{0.084}$) alloy the elastic energy is ~ 4 (2.5) $\times$ that of the buffer, which leads to a slight relaxation of the compressive strain in the GeSn layer following the undercut etch.

Subsequently, disks are coated with a 10–20 nm thick low stress SiN layer that helps promote

Optics EXPRESS

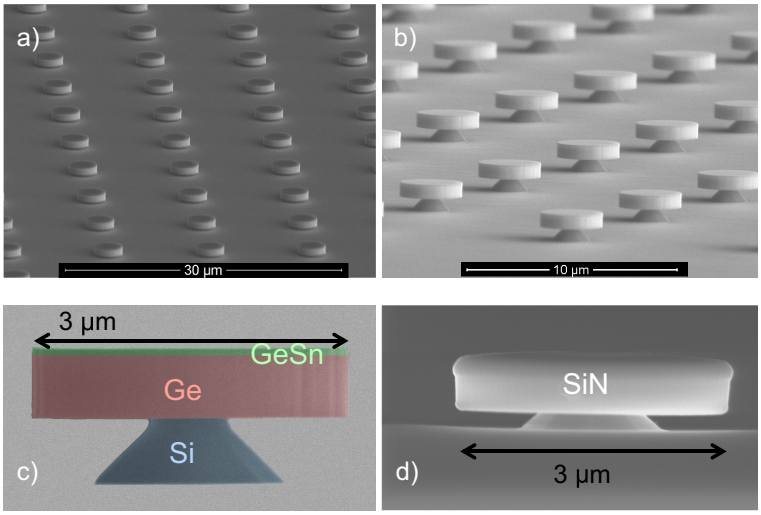

Fig. 3. a) A scanning electron microscope (SEM) image of a dry etched GeSn/Ge disk array. b) GeSn/Ge disk array following a wet etch in tetramethylammonium hydroxide to etch the Si. c) A false coloured SEM image of a 3 μm diameter GeSn/Ge disk, highlighting the materials the disk comprises. d) An SEM image of a high stress silicon nitride coated disk.

adhesion of the SiN stressor. A ~ 300 nm high stress SiN layers is then deposited at room temperature in an inductively coupled plasma (ICP) plasma enhanced chemical vapour deposition (PECVD) tool, Fig. 3(d). While future devices will likely achieve tensile GeSn with the use of SiGeSn VSs, these ternary alloys are still in their infancy. The application of high stress SiN layers is a technique which is highly applicable to creating tensile strained GeSn [29], as other straining techniques previously used for Ge rely on the residual tensile strain in the epilayer [6], which is not present in such alloys. The SiN films in this work have compressive stresses of ~ 2.3 GPa, as measured using the curvature technique [30]. When deposited on a μ–structure, the compressive stress in the film relaxes and transfers tensile strain to the underlying feature [10]. Opposed to previous work with SiN stressors [29], which used GeSn quantum wells, we investigate pseudomorphic layers at the top of the disk structure,which allows for a much larger strain transfer from the SiN stressor. This design, in conjunction with Sn contents up to 10.7 %, allows us to explore low defect GeSn layers that are direct bandgap by up to 85 meV, and emit in the MIR.

4. Strained GeSn

Fabricated samples were investigated by room temperature PL, using a Bruker Vertex 70 Fourier-transform infrared (FTIR) system, with a liquid nitrogen cooled InSb detector. A 532 nm excitation source was used, in conjunction with a longpass filter to reject the pump into the spectrometer. The laser was mechanically chopped, and the system was operated in step-scan mode to remove ambient blackbody radiation from the spectra. Following initial investigations, it was found that an additional passivation layer between the GeSn and the SiN is crucial to achieving bright PL. Here, the SiN layers have not been optimised for passivation, and therefore these observations are not intended to be a conclusive comment on the passivation of GeSn with SiN. The results, however, have been included for transparency. In order to clearly observe PL emission, an intermediate passivation layer was therefore required. In particular, Al_2O_3 layers deposited by atomic layer deposition were investigated, which have previously shown low density of interface traps to GeSn alloys [31]. The deposition of a 20 nm Al_2O_3 layer alone did not

Optics EXPRESS

increase (nor decrease) the intensity compared to the bare disk, suggesting that PL intensity enhancements could be realised with an optimised passivation process [31], however it clearly mitigates the poor electronic interface caused by the stressor. This can be observed in Fig. 4(a), which shows the unstrained emission, compared to strained 3 μm diameter $Ge_{0.893}Sn_{0.107}$ disks, with and without Al_2O_3 layers. In future, a greater understanding of the thermal budget of GeSn layers will facilitate the development of an optimized anneal processes to improve passivation.

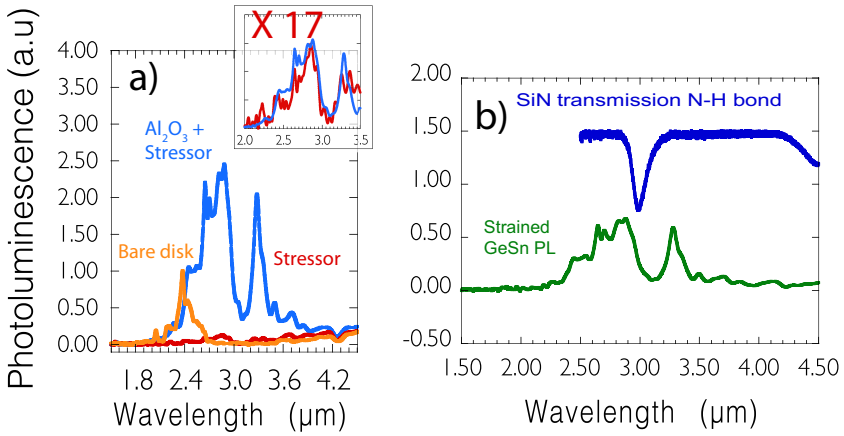

Fig. 4. a) Photoluminescence (PL) from $Ge_{0.893}Sn_{0.107}$ alloys. Compares the PL from bare undercut disks, to disks with and without Al_2O_3 passivation with SiN stressors. b) PL from strained $Ge_{0.893}Sn_{0.107}$ disk, with silicon nitride transmission over-layed. The transmission is scaled and offset for clarity. The dip shown at ~ 3 μm relates to the N-H vibration.

A clear intensity increase and red-shift is observed for the strained and passivated structures, which are hallmarks of tensile strain. As in Fig. 4(a), it appeared that two peaks are present in the in PL, which were initially considered to be from valence band splitting under tensile strain, with the long wavelength peak stemming from $\Gamma \rightarrow$ light-hole (LH) transitions. This has instead been identified to be absorption and/or scattering from the N-H stretching bond in the high stress SiN layer. The transmission of the SiN is shown in Fig. 4(b), which has been offset and scaled for clarity. The abrupt change in the refractive index around the molecular vibration, coupled with absorption from this bond is thought to explain the dip in the PL intensity at these wavelengths. Transmission measurements on an FTIR spectrometer system have shown absorption coefficients > 5000 cm^{-1} from the N-H bond in high stress SiN layers. This suggests that a large fraction of the PL intensity could be obscured. It was verified by mid-infrared transmission measurements using an internal glow-bar that no water absorption was present in this spectral region. Weak absorption was visible between 2.6 and 2.8 μm at high resolution, however this was limited by desiccants in the system which keep humidity below 5 %.

Strained microdisks with diameters ranging from 10 – 3 μm were fabricated using both $Ge_{0.916}Sn_{0.084}$ and $Ge_{0.893}Sn_{0.107}$ alloys, and including Al_2O_3 passivation. The room temperature PL from these structures is presented in Fig. 5(a), which compares disks of equivalent Sn concentration and diameter, with and without a SiN stressor. Consistent with previous results on Ge microdisks [13], the strain is increased for disks of smaller diameter, and a clear trend in the PL red-shift is observable. In Fig. 5(a), there is the clear emergence of a long wavelength peak for the $Ge_{0.893}Sn_{0.107}$ samples, and this progression in the PL appears to be consistent with red-shifting PL moving through a constant absorption or scattering process near 3.1 μm. Despite there being a region of the spectra obscured, emission can clearly be observed to extend beyond 3 μm wavelength, significantly into the 3 – 5 μm sensing window. This significant red-shift highlights the extent to which strain engineering can tune the band-edge in GeSn light

Optics EXPRESS

emitters. This work therefore constitutes emission at a longer wavelength than has previously been demonstrated with GeSn, and with a significantly lower Sn content. In [17], Stange et al showed room temperature (RT) PL up to 2.9 μm from partially relaxed GeSn disks with 12.5 % Sn. Previous demonstrations of GeSn layers with Sn concentrations ~ 11 % have shown room temperature PL at ~ 2.4 [16], and 2.5 μm [18] wavelength. Both of such layers had residual compressive strain from growth. This comparison highlights the advantage of our approach, as keeping Sn concentrations to a minimum is advantageous for integration. It should also be noted that recent molecular beam epitaxy (MBE) growths have obtained GeSn layers with Sn contents up to 18 %, [32], however PL spectra were not shown so a comparison cannot be made.

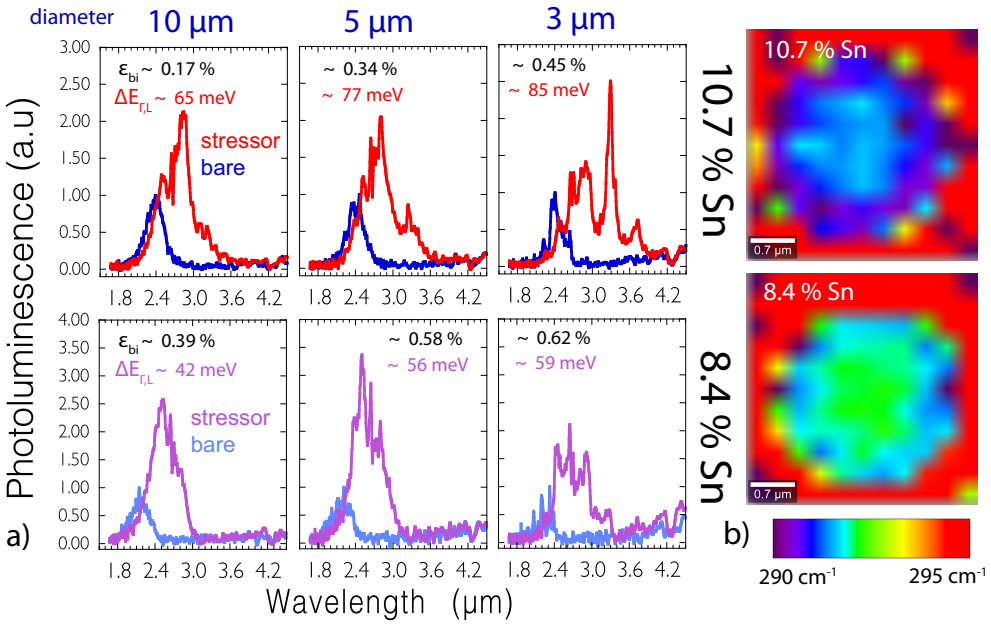

Fig. 5. a) Photoluminescence (PL) from $Ge_{0.916}Sn_{0.084}$ and $Ge_{0.893}Sn_{0.107}$ microdisks with and without SiN stressor layers, for a range of disk diameters. The calculated Γ- to L-valley energy difference is shown for each diameter and Sn concentration, along with the measured strain by Raman spectroscopy. b) Raman maps of 3 μm diameter GeSn/Ge disks with SiN stressors. Both $Ge_{0.916}Sn_{0.084}$ and $Ge_{0.893}Sn_{0.107}$ 3 μm diameter microdisks are shown.

For all samples, an increase in the PL intensity is demonstrated with the addition of strain. The fill factors of each disk array are not constant, therefore the intensities have been normalised to the peak intensity of the unstrained PL for each disk diameter. The relative PL increase for the strained 3 μm 8.4 % Sn sample appears reduced compared to larger diameters; this is due in part to the normalisation to the peak intensity of sharper resonances due to whispering gallery modes (WGM). While such modes are supported in all structures, a clear set of evenly spaced modes was only observed in the smallest structures; this has been attributed to the fact that higher order modes have been cut-off, coupled with enhanced scattering to the surface normal direction due to lower optical confinement. Particularly when comparing the unstrained structures, cavity resonances can be seen to modulate the spectra; likely from both Fabry-Perot and WGM.

In order to quantify the strain of the disks Raman maps were taken across all disk diameters for both alloys, Fig. 5(b). A confocal Raman microscope was used, with a 100 X 0.9 NA objective, and a 532 nm excitation source. The laser is absorbed in approximately the top 20 nm of the disk and therefore probes the strain at the top surface. Further details of this measurement are given in previously published works [10, 13]. As with similar structures [13], a trend of increased strain

Optics EXPRESS

towards the disk edge was observed in maps, with minimum strain transfer directly above the Si post. As discussed in ref. [13], finite element modelling shows the disks are predominantly biaxially strained, with $\varepsilon_{xx} = \varepsilon_{yy}$, and therefore a biaxial approximation has been used for the extraction of the strain from the Raman measurements. A measured strain shift coefficient of ~ 420 cm^{-1} was used to extract the strain, in conjunction with a Sn shift coefficient of 83.1 cm^{-1} [33]. The higher strained regions of the disk should dominate the PL spectra, opposed most commonly measured strain value (statistical mode), however the extent to which each region contributes to the PL depends on a number of unknown parameters, such as the diffusion length of the injected carriers. To approximately attribute a level of strain to each spectra, histograms of the Raman spectral position across the disks were generated, and fitted with Gaussian distributions. The strain value at the 1/e point of the high strain side (low frequency) of the Gaussian has been displayed in Fig. 5(a) along-side each spectra. The highest strained $Ge_{0.893}Sn_{0.107}$ disks are demonstrated to have tensile strains of ~ 0.45 % accounting for a ~ 1.9 % change in strain from the as grown structure to the disk with a stressor.

Using the value of strain measured by Raman, the Γ to L energy differences were calculated according to deformation potential theory, and are also presented in Fig. 5(a). A linear combination of Ge [14] and Sn [16] deformation potential contants were used, in conjunction with the bandgap bowing and Sn parameters reported in [16]. All of the tensile strained alloys are significantly direct, with the Γ-valley calculated to be 85 meV lower than the L-valley for the highest strained 10.7 % Sn disks. This a key metric for achieving room temperature lasing or efficient light emission, as a larger Γ to L difference (i.e. E_L - E_Γ), leads to an increased carrier concentration in the Γ-valley and therefore an increased quantum efficiency. Significantly, the energy difference calculated here is larger than the GeSn lasers demonstrated so far [16–18], even with a lower Sn concentration. Such techniques should therefore enable lasers to be achieved with reduced thresholds.

5. Low temperature PL

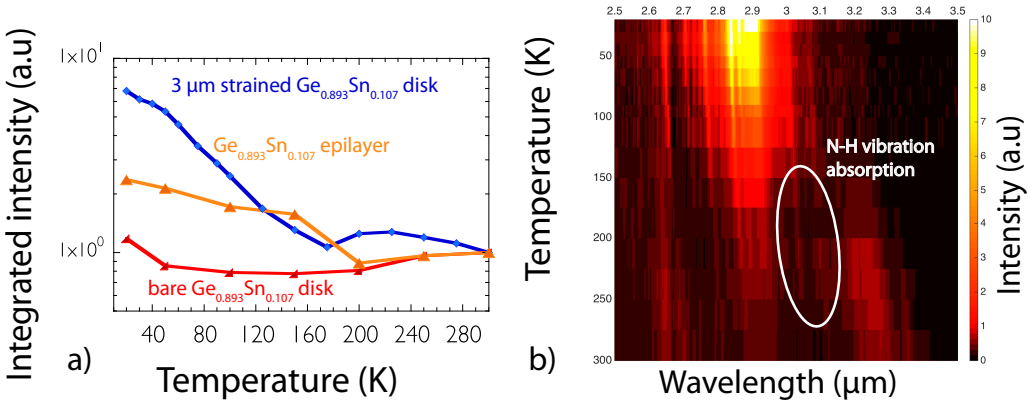

Fig. 6. a) Integrated photoluminescence (PL) intensity of $Ge_{0.893}Sn_{0.107}$ layers. A bare 3 μm, unpassivated disk is shown, as well as the as grown epilayer, and the strained $Ge_{0.893}Sn_{0.107}$ disk with ~ 0.45% tensile strain. b) PL intensity colour map, as a function of wavelength and temperature, for the 3 μm $Ge_{0.893}Sn_{0.107}$ disks with ~ 0.45 % tensile strain.

Low temperature PL measurements were carried out on all disk samples. Measurements were undertaken in the range of 300 - 20 K, using a closed cycle optical cryostat. As discussed previously, these measurements can be used to identify direct bandgap behaviour. Figure 6 demonstrates the low temperature PL for the 3 μm $Ge_{0.893}Sn_{0.107}$ microdisks, and the integrated intensity

Optics EXPRESS

is shown for disks with and without stressor layers. Contrasting behaviour is clearly observed, with the unstrained disk demonstrating minimal sensitivity to temperature. Interestingly, this is a different temperature dependence to the as-grown epilayer. It is believed that the introduction of surface states from the dry etch is responsible for this change in behaviour resulting in a higher density of non-radiative recombination centres. In comparison, the strained disk demonstrates a larger increase at low temperature than both the as-grown alloys and the bare disks. For the 3 μm $Ge_{0.893}Sn_{0.107}$ samples, there is just under a 7 $\times$ relative intensity increase at 20 K compared to 300 K. This relative intensity increase is significantly less than the relative increase in direct bandgap layers in shown by Wirth et al [16], however, this cannot directly be compared due to a significant difference in dislocation densities [20]. Here, the contrasting behaviour compared to the unstressed disks, coupled with the long wavelength emission from strain, is indicative of a direct bandgap semiconductor.

The low temperature PL behaviour shown in Fig. 6(b) is further evidence that the two peaks observed in Fig. 4 and 5(a) do not relate to separate Γ to valence band transitions but rather a molecular absorption line. If a split valence band had been responsible for the spectra, it would have been expected that the longer wavelength peak would dominate the spectra at low temperature; as the injected holes would primarily populate the upper valence band. Here, the low temperature PL is more consistent with the spectra blue-shifting into an absorption band, as the bandgap increases at low temperature. This can be clearly observed in Fig. 6(b), which demonstrates the PL intensity as a function of temperature and wavelength. The long wavelength peak can be observed to disappear below 200 K, with strong PL emerging at $\sim$ 2.85 μm at 20 K. This also reinforces that a portion of the spectra is obscured, and may therefore affect the accuracy of the integrated intensity vs temperature, Fig. 6. A similar trend was observed with $Ge_{0.916}Sn_{0.084}$ disks, which demonstated a relative intensity increase of approximately 3.6 $\times$ the room temperature PL. This is suggestive that the PL intensity does somewhat scale with the Γ- to L-valley energy difference. Arrhenius plots were examined and it was found activation energies were significantly lower than the expected Γ to L-valley energies, suggesting that the thermal quenching is dominated by another shallow impurity state. For example, from 300 K to $\sim$ 50 K an E_a of $\sim$ 17.5 meV is extracted. As stated previously, however, the obscured region of the spectra could introduce error to this calculation.

6. Discussion

In this work, it has been shown that strain engineering can be used to create a direct band structure, with pseudomorphic layers and Sn contents below 11 %. An important point is that this alleviates the need for plastic deformation, and the associated defect density. This can be crucial to improved quantum efficiencies, and it has been previously shown in Ge that reducing dislocation densities can have orders of magnitude of effect on the PL emission intensity [19] [34]. With defects minimised, the internal quantum efficiency here is expected to be predominantly limited by surface recombination velocities, which can be reduced by an optimised passivation process. Regardless of Sn content, these techniques can provide a tuneable emission wavelength or improved light emission properties from a single epitaxial growth step. Tensile strain also relaxes the need for high Sn contents, which can reduce thermal budgets and make integration challenging. It is acknowledged that high Sn content SiGeSn layers are very promising candidates as buffers for growth of tensile GeSn, such ternary alloys, however, have many technical challenges, and the techniques here therefore demonstrate a practical means of investigating tensile GeSn layers.

Furthermore, this type of structure could be of interest for a number of applications where lasing is not a requirement. With the emission extending past 3 μm wavelength, there are a number of molecules which could potentially be detected using tensile strained GeSn as an optically pumped source. The emission from the 3 μm $Ge_{0.893}Sn_{0.107}$ microdisk most closely overlaps with methane absorption lines. Data from the HITRAN database was used to model the emission

Optics EXPRESS

through a 5 mm path length of 5 % methane at atmospheric pressure [24], and is demonstrated in Fig. 7. For 400 parts per million (ppm) detection, a 0.036 % reduction in the integrated intensity of the spectra would have to be detected, however this could be boosted substantially with a narrowband filter centred around the 3.31 μm wavelength absorption peak. In the absence of an electrically contacted device, there is the potential to use low cost, commercially available, visible laser diodes to optically pump the GeSn MIR microdisks on a Group IV platform, opposed to using III-V or quantum cascade laser (QCL) systems. The use of 40 nm thick pseudomorphic layers does not inhibit bright PL emission, as all of the 532 nm source is absorbed in the top 20 nm of the structure, and a type 1 band alignment at the Γ-valley reduces carrier diffusion to the Ge. This, combined with a low defect, direct bandgap active region can allow for bright PL. Further work is required to quantify the quantum efficiency.

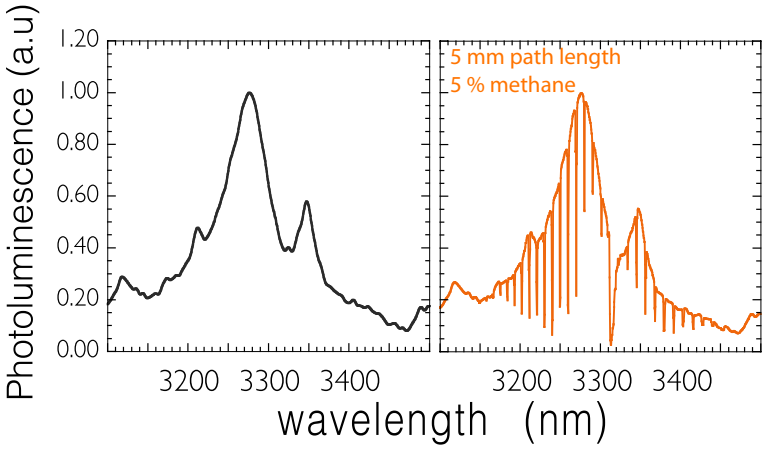

Fig. 7. Left - Photoluminescence of the long wavelength emission from $Ge_{0.893}Sn_{0.107}$ disks. Right - Simulation of the spectra having propagated through 5 mm of 5 % methane (CH_4) at atmospheric pressure.

In order to reach further into the MIR and cover the entire 3–5 μm window, there are alternative approaches. For example, 12.6 % alloys with 1 % tensile strain could reach as far as 5 μm wavelength. This of course would rely on partial relaxation from thicker layers, which brings a trade-off with an increased defect density. Higher Sn concentrations could also be used in pseudomorphic layers.

With regard to lasing, in the devices demonstrated here the optical overlap of the propagating mode is expected to be < 5 %, with most light propagating in the transparent Ge buffer. The combination of a low modal overlap and low injection ($\leq$ 1 kW/cm^2) has limited the exploration of lasing in this work. To enable lasing, future design trade-offs can be made between the alloy thickness, the dislocation density, the strain profile and the optical overlap, in order to engineer lasers operating above 3 μm. It is expected that the active GeSn region will be required to be in the upper-most part of the Ge disk (i.e. above centre) to achieve sufficient tensile strain [28] [13].

7. Conclusion

GeSn alloys were grown pseudomorphically on Ge buffers on Si substrates, which demonstrated no strain relaxation by XRD and therefore have low dislocation densities. The alloys as-grown were calculated to be indirect bandgap, and the temperature dependent PL was found to be consistent with high quality, indirect GeSn heterolayers. Undercut GeSn/Ge microdisks were fabricated using Si foundry compatible processes, and strained by SiN stressor layers. It was found that the addition of ALD deposited Al_2O_3 layers significantly enhanced the quantum efficiency,

Optics EXPRESS

compared to disks with only SiN stressors. A range of disk diameters were used to demonstrate an increasing progression in the red-shift of the PL, and it was found that part of the emission is obscured by an absorption band, identified as the N-H stretching vibration in the SiN film. Nevertheless, clear direct bandgap emission could be observed significantly past 3 μm wavelength, the longest wavelength demonstrated by GeSn light emitters to date. Furthermore, according to deformation potential theory, these layers demonstrate a larger energy difference between the Γ- and L-valleys than previously demonstrated GeSn lasers. The temperature dependence of the strained devices demonstrated contrasting behaviour to unstressed the GeSn/Ge microdisks, further highlighting the change from indirect to direct bandgap through the application of tensile strain. It is demonstrated by simulation that the long wavelength emission from $Ge_{0.893}Sn_{0.107}$ microdisks overlaps with the methane absorption spectra, which highlights the potential for tensile strained GeSn technologies to be used for Group IV compatible gas sensing on a Si platform.

Funding

U.K. EPSRC (EP/N003225/1).

Acknowledgments

The authors thank the staff of the James Watt Nanofabrication Centre for help and support in undertaking the research.